

# ST-ECF Newsletter

ESA & Garret Mellema  
(Leiden University, The Netherlands)

*The Red Spider Nebula, NGC 6537, is a striking 'butterfly' or bipolar planetary nebula. This NASA/ESA Hubble Space Telescope image shows that the gas walls of the two lobed structures are not smooth, but rippled in a complex way. These waves are driven by stellar winds radiating from the hot central star. The image was created from exposures through five different filters: ionised sulphur (red), ionised nitrogen (orange), ionised hydrogen (green), atomic oxygen (light blue) and ionised oxygen (dark blue).*

Read more at <http://hubble.esa.int> under "Releases" (heic0109)

## HST NEWS AND STATUS

*Jeremy Walsh*



Preparations are well advanced for the next HST servicing mission, SM3B, which will include the installation of the first new scientific instrument on HST for five years, the Advanced Camera for Surveys (ACS), and the restoration of the performance of the NICMOS infrared instrument by the installation of a cryocooler.

The launch of SM3B is currently planned for late February 2002 and the mission should last 11 days, including a total of five EVAs. Highest priority for the continued life of HST is the installation of new Solar Arrays, similar to those used in the Iridium satellites. The other top priority item is the replacement of the Power Control Unit (PCU) that controls the battery charging. There is a possible failure path for this unit that would leave HST without power. Therefore the unit must be replaced by the astronauts, even though it was not designed as a replaceable item. The Advanced Camera for Surveys (ACS) will be installed in the bay freed by the removal of the ESA Faint Object Camera (FOC) and the NICMOS cryocooler will be attached to enable the cooling of the three NICMOS detectors to about 80K. Although warmer than the design operating temperature, the overall sensitivity of NICMOS will only be slightly degraded since the higher detector dark current is partially offset by higher detector quantum efficiency. This will be HST's only IR capability until the installation of the WFC3 in SM4. It is still undecided whether the Rate Sensing Units (gyros) will be replaced. Gyro#5 has failed and the companion in the same unit (#6) has shown a problem. Another gyro (#3) showed a "lube patch event" (caused by solidification of lubricant) in November and is therefore suspect. Three gyros are required for full HST attitude control so the prospects for full control through the two years to the next servicing mission look uncertain.

Looking back to recent significant events, STIS was returned to full operating status in early August 2001 after the electronics and power supply were transferred to the redundant Side 2. The cause of the failure of the Side 1 power supply, which had been operating in-orbit since Servicing Mission 2 in February 1997,

was determined to be a short circuit in the low voltage power supply. Whilst the UV MAMA performance was unaffected by the change, the CCD read noise showed an increase from 4.4 to 5.4 electrons. This degradation will only affect those programmes performing spectroscopy on faint extended objects. The Side 2 electronics were known to have a faulty CCD temperature sensor before launch, so more monitoring is now required to manage the result of the changes in temperature of the CCD housing. Temperature dependent dark exposures are required and will be enabled in the reduction pipeline. STIS has thus been returned to nominal status; however there is no spare for Side 2 and STIS is the only general purpose (long slit) spectrometer available for the remaining orbital life of HST.

In mid-November, the HST Cycle 11 Time Allocation took place. Cycle 11 saw the introduction of several new proposal categories — Treasury, Legacy Archive and Theory. The Treasury category requires not only that the data be made public, but also that data products (catalogues, etc) be produced and made available to the community. The highly topical areas of millennium astronomy were awarded Large (>100 orbits) and Treasury time — deep surveys, galaxy evolution, gamma-ray bursters, supernovae as cosmological probes, deep stellar-population studies and Kuiper belt objects. About 30% of the Cycle 11 allocation was devoted to these proposals. There were 11 subject panels, including Solar System, who allocated the remaining ~1800 Cycle 11 orbits to proposals in the 1-99 orbit category. The panels tended to favour smaller proposals, perhaps as a counter to the large number of orbits taken by the Large and Treasury programmes. European proposal submission was above the input level for Cycle 10 (22.0% by number, 18.7% by orbit in Cycle 11 as against 16.6% and 17.7% respectively in Cycle 10). The success statistics have also improved, with 19% of successful proposals in Cycle 11 having an ESA affiliated PI, reversing a trend seen since Cycle 8. Not surprisingly the most popular instrument will be ACS, with 58% of GO programmes. The first ACS images are eagerly awaited.



## NGST NEWS

*Bob Fosbury & Peter Jakobsen (ESTEC)*



In October 2001 the Phase 2 proposals for the NGST Observatory were submitted to NASA. The proposals are now being reviewed and we expect to learn the identity of the selected industrial prime contractor during the first quarter of 2002. Also during the autumn, NASA issued the Announcement of Opportunity (AO) for four different science investigations that will utilise the NGST (see <http://ngst.gsfc.nasa.gov/>). These are:

- to develop and use scientific instrumentation capable of achieving the imaging goals of NGST in the near infrared (NIR: defined as 0.6-5 microns) wavelength regime;
- to participate in the development, integration and testing of the facility mid-infrared (MIR: defined as 5-28 microns) instrument (MIRI) in addition to using data from the instrument

(MIRI Science Lead investigations and MIRI Science Team Member investigations);

□ to conduct interdisciplinary investigations using data taken by the reference observatory and reference instrument set, as well as actively participate in NGST facility and telescope development (Facility Scientist investigations and Telescope Scientist investigations);

□ to conduct interdisciplinary investigations using data taken by the reference observatory and reference instrument set and participate in the science oversight of the NGST development (Interdisciplinary Scientist [IDS] investigations).

The proposals for these opportunities are due at NASA in March 2002 with the goal of making a selection in June.

The first of these, NIRCam, is to be constructed with the participation of the Canadian Space Agency (CSA).

The US half of the MIRI project will be implemented by a team from the Jet Propulsion laboratory (JPL) who were recently selected from proposals submitted by NASA centres. The other half of the instrument is to be provided by a group of ESA member states in Europe coordinated by the Agency. ESA have just awarded a study contract to the consortium that is lead by the UK Astronomy Technology Centre (ATC) in Edinburgh. The kick-off meeting for this study was held at ESTEC in early December 2001 and was attended by the European MIRI Study Consortium, the JPL MIRI Study Team, the GSFC NGST Project, STScI, Air Liquide (the contractor selected to study the MIRI cryostat), and ESA (including the ST-ECF).

The principal scientific instrument to be supplied by ESA, the NIR spectrograph, NIRSpec, has been the subject of a number of European industry/academia feasibility and assessment studies during the last two years. This process culminated during a week of final study presentations held at the ST-ECF in Garching in mid-November 2001. The project will now proceed to a one-year Phase-A study carried out by two competing consortia that have Astrium and Alcatel as their leading industrial components. Closely allied with this process is the development of the micro-mirror or micro-shutter (MEMS) devices that are the preferred slit-selection mechanisms for this highly spatially-multiplexed spectrograph. A broadly-based MEMS review board has been constituted that has the task of advising NASA which of the three research programmes currently underway in the USA (at GSFC and at the Sandia National Labs) should be selected for further funding before a MEMS go/no-go decision point is reached in 2003. In case a suitable device does not reach the required readiness by then, ESA is continuing the development of a more conventional mechanical slit-selection system as a back-up. A number of critical performance parameters associated with this type of spectrograph, notably the contrast between selected and non-selected objects and the calibration accuracy, have been evaluated by both the consortia and the ESA Study Science Team (SST) in collaboration with the ST-ECF.

Finally, the planning for the scientific operation of the NGST Observatory is proceeding with the STScI, the NASA-nominated Science Operation Center, currently preparing a detailed proposal. ESA is also engaged, through both STScI and the ST-ECF, in planning its own contribution to Science Operations. The principal areas for ESA will logically concern instrument science activities for NIRSpec and, possibly, some similar aspects of MIRI.



#### First image of a Dark Matter object

*This NASA/ESA Hubble Space Telescope image is based on three exposures from the WFPC2 camera obtained in the V, R and I bands - shown as blue, green and red respectively. It includes the first image of a Dark Matter object — a MACHO (a massive compact object) — the red object indicated with an arrow. This MACHO is a nearby red dwarf star that gravitationally focused light from a blue background star in another galaxy (seen just to the left of the MACHO) in a so-called microlensing event. Since the event six years ago, the MACHO has moved 0.134 arc-seconds on the sky and can now be clearly separated from the blue star in the image.*

*The result is strong support for the theory that a large fraction of baryonic (ordinary) Dark Matter exists as small, faint stars in galaxies such as our Milky Way.*

Read more at <http://hubble.esa.int> under "Releases" (heic 0116)



# THE IN-ORBIT WAVELENGTH CALIBRATION OF THE ACS GRISM

*A. Pasquali, N. Pirzkal & J.R. Walsh*

The Advanced Camera for Surveys (ACS) will increase the discovery efficiency of HST by offering both larger detector area and higher spatial sampling than any current HST instrument. ACS features three independent cameras that can be used for both imaging and spectroscopy:

□ The Wide Field Channel (WFC) performs imaging and grism, slitless spectroscopy from optical wavelengths to 1 micron, over a  $3.4' \times 3.4'$  field of view with a sampling of  $0.05''/\text{pix}$ .

□ The High Resolution Channel (HRC) features near-UV to 1 micron imaging, near-UV to optical prism slitless spectroscopy and visible to one micron grism slitless spectroscopy. The HRC field of view is  $26'' \times 29''$  with a pixel size of  $0.025'' \times 0.028''$ .

□ The Solar Blind Channel (SBC) provides far-UV imaging and prism slitless spectroscopy. The SBC field of view is  $31'' \times 35''$  with a pixel size of  $0.030'' \times 0.034''$ .

The first order grism dispersions are  $40 \text{ \AA}/\text{pix}$  and  $25 \text{ \AA}/\text{pix}$  for the WFC and the HRC, respectively and the corresponding values in the second order are  $20 \text{ \AA}/\text{pix}$  (WFC) and  $12 \text{ \AA}/\text{pix}$  (HRC).

The ST-ECF is responsible for the support of the spectroscopic modes of ACS. This work includes the provision of the SLIM simulator and the aXe spectrum extraction software that have both been described in detail in the previous two ST-ECF Newsletters and elsewhere. This article describes plans for the in-orbit wavelength calibration of the ACS spectral modes.

## TARGET SELECTION

The dispersion and instrumental PSF define the maximum spectral resolution of the ACS grism and prisms, but this is significantly degraded when extended sources are observed. The effect is exacerbated by the high spatial resolution of the ACS. One way to illustrate this effect is by simulating emission-line objects with varying sizes, shapes and orientations on the sky (cf. Pasquali et al. 2001a). These simulations were performed using the spectrum of the Galactic Planetary Nebula NGC 7009, scaled down in flux by a factor of 30 to avoid CCD saturation in a 1 second exposure (cf. Pirzkal et al. 2001).

Here we focus on the results obtained for the WFC, but similar conclusions would be reached using simulated HRC data. The first order grism spectra obtained for the WFC are shown in Figure 1: Figure 1a contains the spectra of a disc-shaped source, and Figure 1b the spectra of an elliptical nebula. Line blending becomes important for object diameters larger than two pixels ( $0.1''$  and  $0.05''$  for the WFC and HRC, respectively) and as the object major axis aligns with the dispersion axis ( $PA < 45$  degrees) for elliptical sources.

In the planning of the in-orbit wavelength calibration of the ACS grism, the targets should have a small size to allow accurate determination of the wavelength calibration. Pasquali et al.

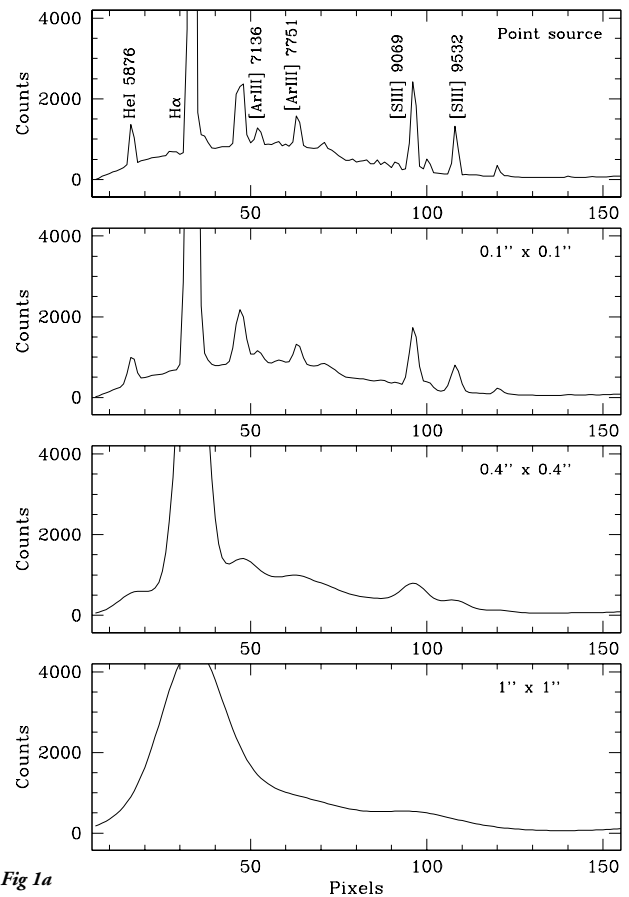


**Fig 1a**

**Fig 1a and 1b:** SLIM simulated WFC 1st order grism spectra of NGC 7009 obtained by: a) increasing the diameter of a disc-shaped PN and b) rotating the major axis of an elliptical nebula ( $0.1'' \times 0.25''$  in size) from perpendicular ( $PA = 90$ ) to parallel ( $PA = 0$ ) to the image X axis. Exposure time is 1 second and no background has been added.

2001b gives a more detailed discussion of the effects of image size on the spectral resolution of the ACS.

In addition, targets should be selected so that:

- their brightness allows relatively short exposure times (less than one orbit);
- their spectra present a significant number of well separated emission lines;
- they should not be associated with extended nebulosity that could degrade the spectral resolution of the grism and increase the local background;
- their variability is negligible so that their emission lines can be identified at different epochs;
- they do not lie in crowded fields to avoid overlapping spectra and contamination;
- they should be visible for as much time as possible (ideally in the continuous viewing zones) to allow repeated HST visits at any time.

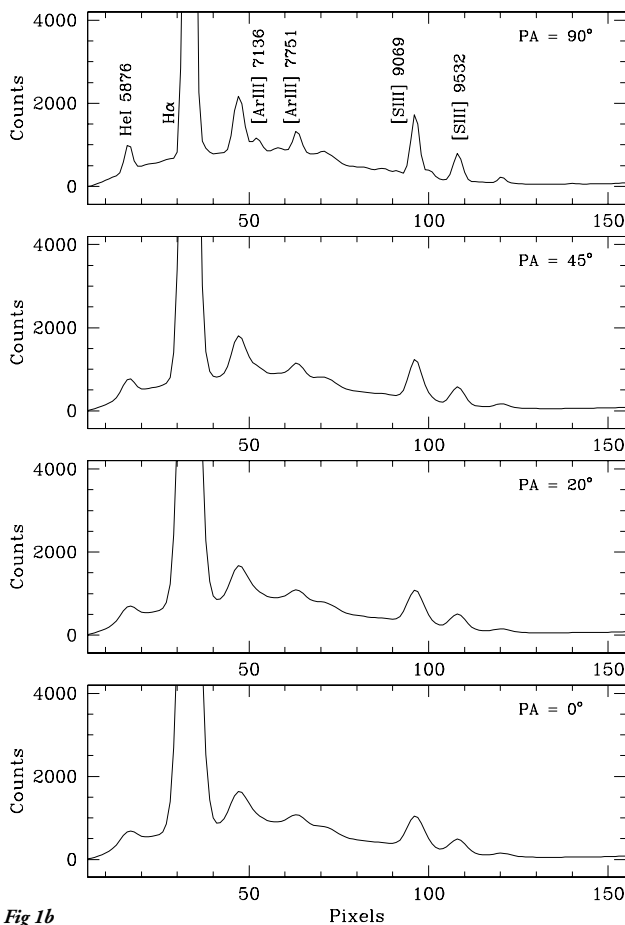


Fig 1b

### PLANETARY NEBULAE?

The obvious choice for wavelength calibrators would be Planetary Nebulae (PNe) because of their many strong emission lines and weak continuum. Due to the caveats on the grism spectral resolution previously discussed, they should neither be Galactic nor located in the Magellanic Clouds since these PNe are rarely compact (apparent size  $< 0.1''$ ) when imaged with HST and are often surrounded by a low intensity halo. PNe in M31 could be compact enough, but are unlikely to be bright enough.

To test this possibility the spectrum of the Galactic PN NGC 7009 was scaled to the  $H\beta$  flux measured for CJFN #31 in M31 (Jacoby and Ciardullo 1999). SLIM grism spectra simulating this object as observed with the WFC and the HRC were generated. The results are plotted in Figure 2. The adopted exposure times are 1200s and 2400s for the WFC and the HRC, respectively. The WFC grism 1st and 2nd orders are shown in the top panels, while those obtained for the HRC are shown at the bottom of Figure 2. Clearly, the number of detected emission lines is sufficient to wavelength calibrate only the grism first order. This, and the large exposure times involved, make PNe in M31 unsuitable for repeated grism slitless observations at different positions on both the WFC and the HRC to measure the variation of the dispersion solution as a function of position in the field of view.

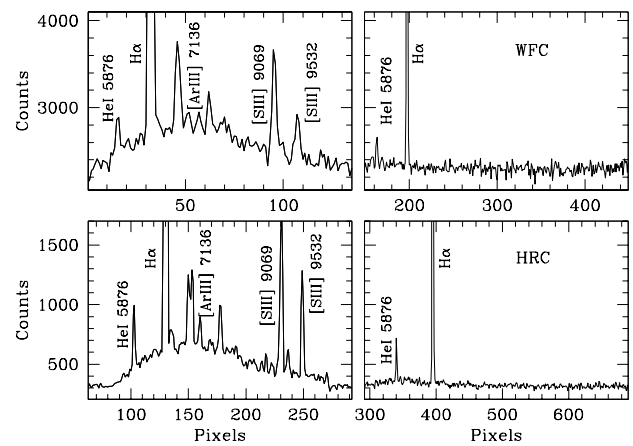


Fig 2: Top: Grism 1st and 2nd order spectra of CJFN #31 as computed for the WFC with an exposure time of 1200s. Bottom: As above, but for the HRC and an exposure time of 2400s. Background and noise have been added.

### WOLF-RAYET STARS

Instead we will pursue an alternative wavelength calibration plan using luminous, point-source emission line objects, such as Galactic Wolf-Rayet (WR) stars (cf. Pasquali et al. 2001b), in particular those classified as WC6 to WC9, which have spectra rich in carbon emission lines (cf. Figure 3).

An important issue here is how the line broadening produced by the WR stellar wind affects the accuracy of the grism dispersion

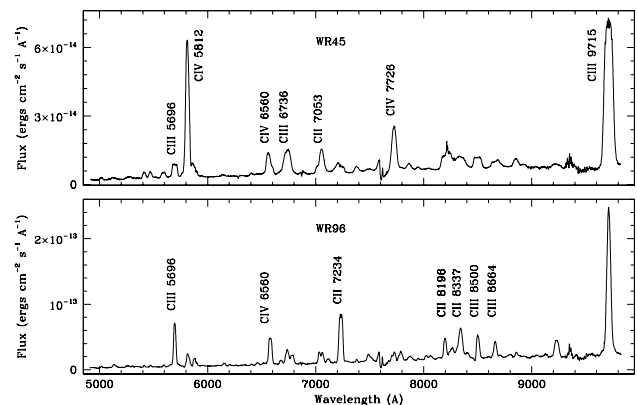


Fig 3: High resolution ( $1.26\text{\AA}/\text{pix}$ ) spectra of WR45 and WR96 obtained with the ESO NTT/EMMI spectrograph (Proposal ID 266.D-5653).

solution. A statistical analysis of “The VIIth Catalogue of Galactic Wolf-Rayet stars” (van der Hucht 2001) reveals that wind velocities range between  $\sim 700$  km/s and  $\sim 3300$  km/s (with very few exceptions as large as 5000 km/s), with a mean value of  $1730 \pm 700$  km/s. Objects with a wind velocity larger than 2100 km/s constitute 19% of the whole sample.

In the case of the WFC, a wind speed of 2000 km/s produces a line broadening of about 1.3 and 1.9 pixels in the 1st and 2nd order respectively (1.9 and 3.3 pixels for the HRC). The WR stellar wind is therefore barely resolved in the 1st order spectra of both channels, and partially affects the grism 2nd orders. This is not optimal, but simply a compromise between compact sources with a large number of emission lines and the nominal spectral resolution of ACS.

We have found two WR stars that appear to match our selection criteria: WR45 (WC6) and WR96 (WC9), which have wind speeds of 2100 and 1100 km/s, respectively. As part of the ESO Director General Discretionary Time programme, we have obtained high-to-medium resolution NTT/EMMI spectra of the stars in the spectral range covered by the ACS grism. The flux and wavelength-calibrated spectra are shown in Figure 3. Figures 4 and 5 show simulations of the same objects when observed by the ACS grism. Both first and second orders are plotted. These spectra have been generated using SLIM and assuming exposure times of 10s and 60s in the case of the WFC 1st and 2nd orders, and 20s and 60s for the HRC 1st and 2nd orders.

The spectra shown in Figures 4 and 5 were used to compute the dispersion solution of the grism for both the WFC and the HRC. This was done by measuring the pixel positions of the identified lines with respect to the position of the object in the

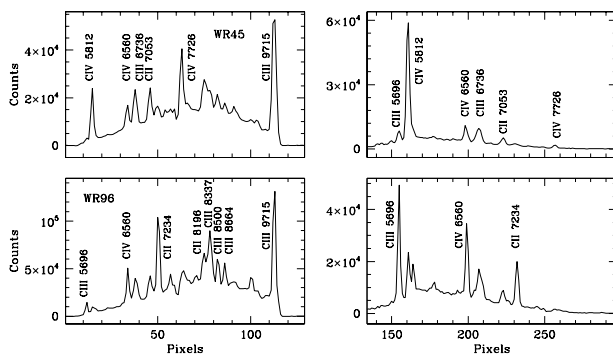


**Fig 4:** The SLIM output spectra for WR45 and WR96, in the case of the WFC. First orders are plotted in the left column and have an exposure time of 10s. The second order spectra are shown in the right column and have been computed for an integration time of 60s.

direct image. These positions were fitted as a function of wavelength using a first order polynomial. The resulting dispersions (for the grism first and second orders in both channels) agree to within 5% of the nominal values. Such an accuracy was achieved with simulated exposure times shorter than 1 minute, ensuring that the observation of WR45 and WR96 can be

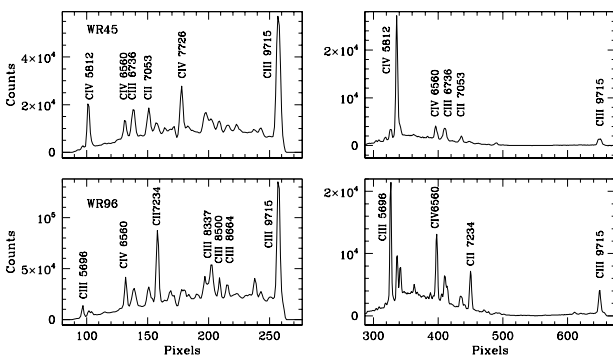


**Fig 5:** The same as for Figure 4, but for the HRC. 1st and 2nd orders have exposure times of 20s and 60s, respectively.

performed at several positions in the field of view to eventually measure the WFC and HRC field variation of the grism dispersion. For these reasons, we have adopted WR45 and

WR96 as the wavelength calibrators of the ACS grism during the SMOV tests. If these observations turn out as expected, then the two Wolf-Rayet stars will also be part of the regular calibration programmes.

## PROPOSED CALIBRATIONS

During the ground tests of ACS, the grism spectrum of a HgAr lamp was acquired at five different positions on the WFC and HRC chips, namely the centre and the edges (close to the CCD amplifiers) of the field of view. Each spectrum was extracted and wavelength-calibrated so that we could derive the grism dispersion and wavelength zero-point as a function of position on the chip. The main result is that the dispersion of the grism first order varies by 25% and 4% across the field of view of the WFC and the HRC, respectively. We believe this to be due to geometric distortion as measured in imaging, and distortions introduced by the grism itself, which is tilted with respect to the surface of the detector.

The SMOV observations have been planned so that the grism spectrum of WR45 will be acquired at the same positions observed during the ground tests. The aim is to derive the in-orbit dependence of the grism dispersion on the position on the WFC and HRC chips and compare it with what is known from the laboratory measurements. Moreover, the SMOV observations will be repeated one week later, in order to check the effects of the filter wheel positioning on the undispersed position of the target on the chip and hence the wavelength zero-point of the grism. It is clear that five positions on the chip are not enough to accurately map the field dependence of the grism dispersion, particularly in the case of the WFC. Therefore, the main purpose of the future calibration programmes will be to extend the grid of positions in the field of view of the WFC and HRC at which WR45 and WR96 will be observed.

## ACKNOWLEDGEMENTS

We would like to acknowledge the ESO Director General Discretionary Time programme and the NTT team who carried out the observations in service mode.



## References

- *Jacoby, G.H., Ciardullo, R., 1999, ApJ, 515, 169*
- *Pasquali, A., Pirzkal, N., Walsh, J.R., 2001b, ST-ECF ISRACS 2001-04 "Selection of Wavelength Calibration Targets for the ACS Grism" (<http://www.stecf.org/instruments/acs/pub>)*
- *Pasquali, A., Pirzkal, N., Walsh, J.R., Hook, R.N., Freudling, W., Albrecht, R., Fosbury, R.A.E., 2001a, ST-ECF ISRACS 2001-02 "The Effective Spectral Resolution of the WFC and HRC Grism" (<http://www.stecf.org/instruments/acs/pub>)*
- *Pirzkal, N., Pasquali, A., Walsh, J.R., Hook, R.N., Freudling, W., Albrecht, R., Fosbury, R.A.E., 2001, ST-ECF ISRACS 2001-03 "ACS Grism Simulations using SLIM 1.0" (<http://www.stecf.org/instruments/acs/pub>)*
- *van der Hucht, K.A., 2001, "The VIIth catalogue of galactic Wolf-Rayet stars", New AR, 45, 135*

# ESA/ESO ASTRONOMY EXERCISE SERIES

Lars Lindberg Christensen & Arntraud Bacher (ESO)



The recently published “ESA/ESO Astronomy Exercise Series” allows students to gain exciting hands-on experience in astronomy by making realistic calculations with data obtained by some of the world’s best telescopes. The students measure and calculate the distances and ages of astronomical objects, among the most basic problems in modern astrophysics, using observations made by the NASA/ESA Hubble Space Telescope and ESO’s Very Large Telescope.

## ASTRONOMY AT THE FRONTLINE OF EDUCATION

The subject of astronomy plays an increasingly important role within education. This is not coincidental — this particular field of basic science is very attractive to young people. Its exploratory and visual nature stimulates youthful minds and the vast expanse of the Universe harbours many unknown secrets just waiting to be discovered. The beautiful and intriguing images brought back by modern telescopes and instruments from the furthest reaches of the Universe are natural works of art that invite contemplation as well as interpretation.

Astronomy is a broad, interdisciplinary field, providing ample opportunities for interesting educational projects covering many different fields of fundamental science, from physics, chemistry and mathematics, to applied research in opto-mechanics, detectors and data handling, and onwards into the humanities.

Reacting to the current need for innovative, high-quality educational material, the European Space Agency (ESA) and the European Southern Observatory (ESO) have collaborated to produce this series of astronomical exercises for use in European high schools.

## IN THE FOOTSTEPS OF SCIENTISTS

The “ESA/ESO Astronomy Exercise Series” has just been made available on the Internet and in printed form. These exercises are designed to give 16-19 year old students exciting hands-on experience in astronomy by making realistic calculations with data obtained by both the NASA/ESA Hubble Space Telescope and

ESO’s Very Large Telescope (VLT). These exercises are carefully prepared by astronomers and media experts and enable the students to measure and calculate fundamental astronomical quantities.

The prime object of the series is to present various small projects that will transmit some of the excitement and satisfaction of scientific discovery to students. By performing the well-structured projects, the students also gain first-hand experience in the application of scientific methods that require only basic geometrical and physical knowledge. They use ideas and techniques described in recent front-line scientific papers and are able to derive results that compare well with those obtained from the much more sophisticated analyses done by the scientists.

## FOCUS ON BASIC THEMES

The first four exercises focus on measurements of distances in the Universe, one of the most basic problems in modern astrophysics. The students apply different methods to determine the distance of astronomical objects such as the supernova SN 1987A, the spiral galaxy Messier 100, the Cat’s Eye Planetary Nebula and the globular cluster Messier 12. With these results it is possible to make quite accurate estimates of the age of the Universe and its expansion velocity, without the use of computers or sophisticated software.

Students can also perform ‘naked-eye photometry’ by measuring the brightness of stars on two VLT images (taken through blue and green optical filters, respectively). They can then construct the basic luminosity-temperature relation (the “Hertzsprung-Russell Diagram”), providing a superb way to gain insight into fundamental stellar physics.

## SIX BOOKLETS

The exercises are now available on the web and in six booklets (100 pages in total), titled: “General Introduction” (an overview of the exercise series), “Toolkits” (explanation of basic astronomical and mathematical techniques), “Exercise 1: Measuring the Distance to Supernova 1987A”, “Exercise 2: The Distance to Messier 100 as Determined by Cepheid Variable Stars”, “Exercise 3: Measuring the Distance to the Cat’s Eye Nebula” and “Exercise 4: Measuring a Globular Star Cluster’s Distance and Age”.

Each of the four exercises begins with a background text, followed by a series of questions, measurements and calculations. The exercises can be used either as texts in a traditional classroom format or for independent study as part of a project undertaken in smaller groups. The booklets are sent free-of-charge to high-school teachers on request and may be downloaded as PDF files from the web site. More exercises will follow in the future.

Contact: [info@astroex.org](mailto:info@astroex.org)

Web site: <http://www.astroex.org>



## DEEP NEAR-INFRARED OBSERVATIONS OF HDF-S

*Eros Vanzella (ESO/Padova), Stefano Cristiani & Collaborators*

In the autumn of 1998 the Hubble Space Telescope observed a small slice of sky in the constellation Tucana for a total of two weeks. The observing strategy of this Hubble Deep Field South (HDF-S) differed from the more famous northern one in several respects. HDF-S consists of a large set of observations of an otherwise unremarkable field around the QSO J2233-606 ( $z = 2.24$ ), taken in parallel by three HST instruments. The Space Telescope Imaging Spectrograph (STIS) was used for both spectroscopy of the QSO and deep imaging. Deep near-infrared imaging was obtained using the Near Infrared Camera and Multi-Object Spectrograph (NICMOS). The Wide Field Planetary Camera 2 (WFPC2) was used to image the main field in a similar manner to the HDF-N observations.

The HDFs represent an major contribution to frontier studies of the distant universe. They have revolutionised the understanding of high redshift galaxies, providing resolved images of faint objects, and contributed in a wide variety of ways to shaping the debate over issues such as the origin of elliptical galaxies and the importance of obscured star formation.

The addition of deep, near-infrared images to the database provided by the HDF WFPC2 data is essential to monitor the SEDs of the objects on a wide baseline and address a number of key issues including the total stellar content of baryonic mass, the effects of dust extinction, the dependence of morphology on the rest frame wavelength, the photometric redshifts and the detection and nature of extremely red objects (EROs).

For these reasons deep near-infrared images were obtained with the ISAAC instrument on the ESO VLT in the Js, H and Ks bands. Figure 1 shows the Ks image and Figure 2 shows a colour composite of the Js, H and Ks frames. The most important characteristics of the infrared observations are given in the Table 1. As a comparison Table 2 lists the corresponding information for the WFPC2 observations (Casertano et al. 2000).

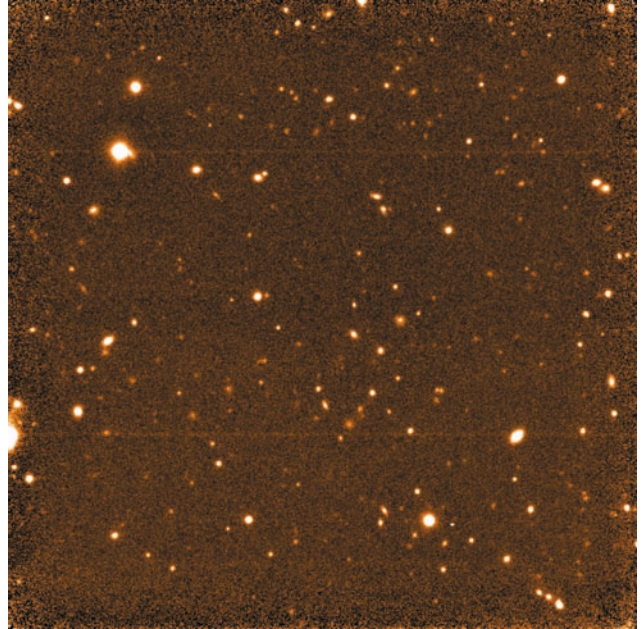


*Fig 1: Co-added VLT/ISAAC Ks infrared image of the HDF-S.*

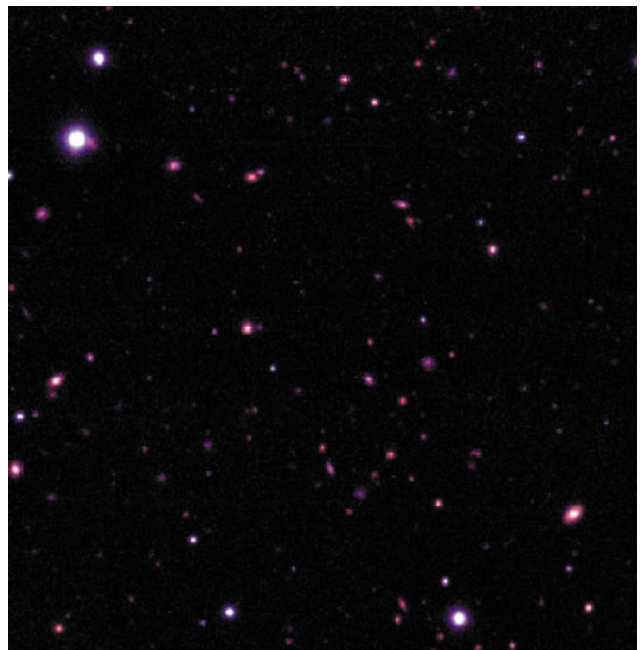


*Fig 2: JHK colour image of the HDF-S. The IR data were obtained with the ISAAC infrared imager/spectrometer (Moorwood et al. 1999) at the ESO VLT-UT1 telescope. The observations were carried out over several nights from September to December 1999 under homogeneous seeing conditions: about 0.6 arcsec. Details of the exposures and limited magnitudes reached are given in Table 1.*

Filter	Wavelength (microns)	Number of frames	Total exp (s)	FWHM (arcsec)	Zero-point	Limiting Mag ( $5\sigma$ )
Js	1.24	210	25200	0.60	28.35	23.5
H	1.65	181	21720	0.60	27.50	22.0
Ks	2.16	487	29220	0.60	26.26	22.0

*Table 1: ISAAC observations. Magnitudes are in the Vega magnitude system.*

Filter	Number of frames	Total exp (s)	FWHM (arcsec)	Zero-point $m_{AB}$	Limiting Magnitude
F300	102	132585	0.16	20.77	26.8
F450	51	101800	0.14	21.9	27.7
F606	49	97200	0.14	23.02	28.3
F814	56	112200	0.14	22.09	27.7

**Table 2:** WFPC2 observations. From Casertano et al. (2000). Limiting magnitudes are  $10\sigma$  AB detections in a  $0.2''$  square aperture.

Even with such very high-quality data the creation of a reliable multi-colour catalogue is not a trivial task. One problem is that the ground-based infrared images have significantly different PSFs than the WFPC2 images. Having in mind the production of photometric redshifts we have developed specific procedures to match HST and VLT data, choosing a conservative approach in the object detection, which has led to a list of 1611 sources.

In Figure 3 the global scheme of the reduction is shown: the SExtractor algorithm (Bertin & Arnouts 1996) has been used for the detection of the sources and the photometry. The catalogue and the infrared images are available at the web page: <http://www.stecf.org/hstprogrammes/ISAAC/ISAAC.html>.

The behaviour of the observed source counts is in general agreement with the result of Casertano et al. 2000 in the Hubble Deep Field South and Williams et al. 1996 in the Hubble Deep Field North, while the corresponding counts in the Hubble Deep Field North provided by Fernández-Soto et al. (1999) are systematically lower by a factor 1.5 beyond  $I_{AB} = 26$ . After correcting for the incompleteness of the source counts, the object surface density at  $I_{AB} \leq 27.5$  is estimated to be 220 per square arcmin, in agreement with the corresponding measure of Volonteri et al. 2000. The estimation of the Extragalactic

Background Light in the I band is consistent with the work of Madau and Pozzetti (2000).

The comparison between the median V-I colour in the Hubble Deep Field North and South shows a significant difference around  $I_{AB} \sim 26$ , possibly due to the presence of large scale structure at  $z \sim 1$  in the HDF-N.

Using the colour-colour diagrams, 90 U-band dropouts have been selected down to  $I_{AB} = 27$  and these are shown on Figure 4. Of these 19 have magnitudes brighter than 25. Spectroscopic observation of the candidates with  $I_{AB} < 24.5$  have been carried out, confirming nine as galaxies with redshifts larger than 2 (marked with red filled symbols on Figure 4). An example spectrum of a  $z = 2.789$  galaxy is shown in Figure 5.

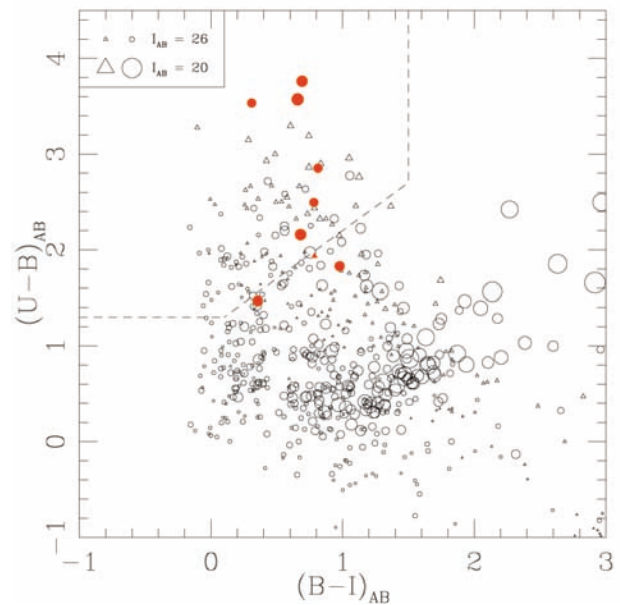


**Fig 4:** Selection of U-band dropouts down to  $I_{AB} = 27$ . Filled symbols represent galaxies with redshifts greater than 2.

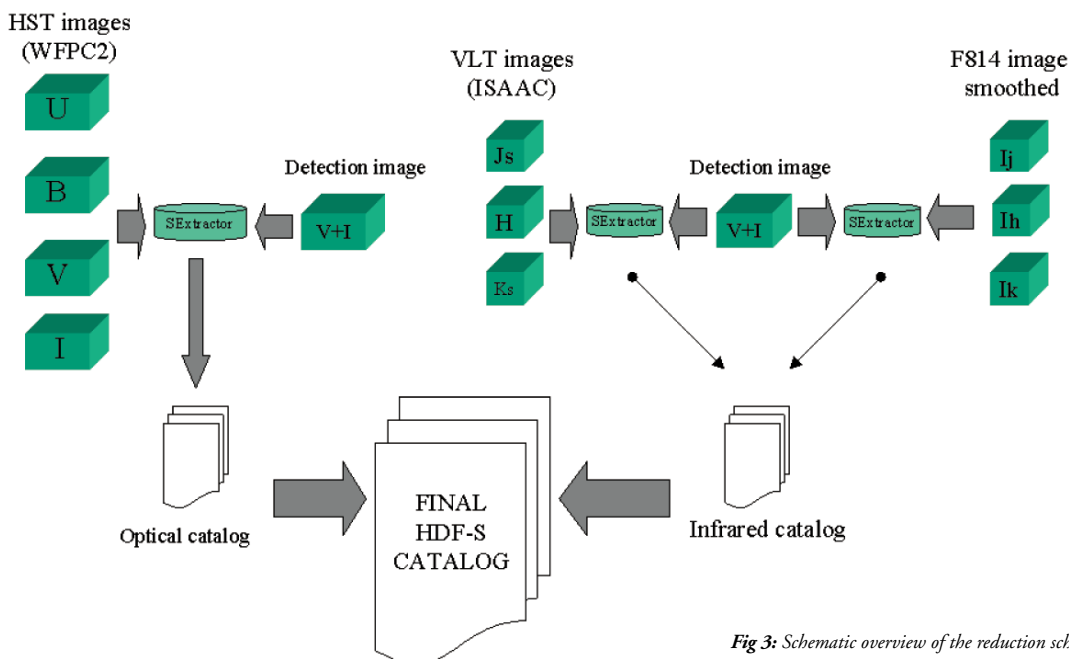


**Fig 3:** Schematic overview of the reduction scheme

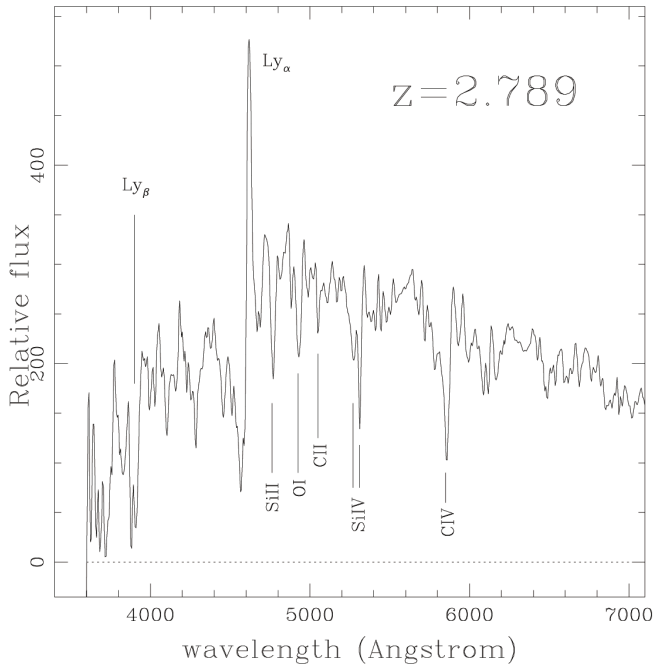


**Fig 5:** Example of a spectrum of a high redshift galaxy, various spectroscopic features typical of a Lyman-Break galaxy are clearly visible.

Similarly, 17 B-band dropouts have been selected down to  $I_{AB} = 27$ . These candidates are typically faint, all with  $I_{AB}$  magnitudes fainter than 26.

Using the deep near-infrared image in the Ks band we have selected a sample of 15 Extremely Red Objects (EROs) defined

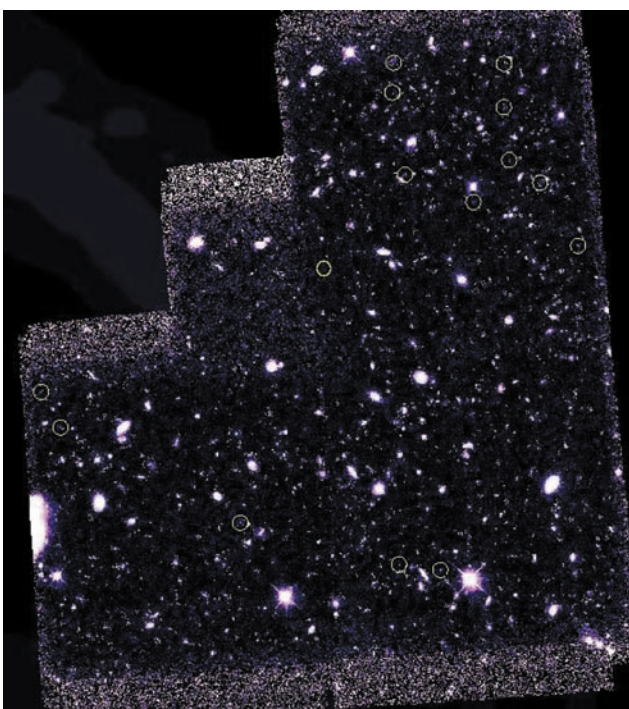


**Fig 6:** The EROs found in the WFC field are marked with circles.

as sources with  $(I-K)_{AB} > 2.7$ , corresponding to the colour of passively evolving elliptical galaxies at  $z > 1$ . The selection was carried out down to  $K_{AB} < 24$ .

The EROs surface density turns out to be  $3.2 \pm 0.9$  per square arcmin, and their distribution in the HDF-S field, at least from the angular point of view, is remarkably nonuniform (Figure 6), 10 EROs out of 15 are inside the upper WFPC2 chip (0.6 square arc-minute). One of the EROs is a powerful radio-galaxy (Norris et al. 1999).

#### The Full Science Team

*Eros Vanzella, ESO/Padova*  
*Stefano Cristiani, ST-ECF/Trieste*  
*Paolo Saracco, Brera*  
*Stephane Arnouts, ESO*  
*Simone Bianchi, ESO*  
*Sandro D'Odorico, ESO*  
*Adriano Fontana, Roma*  
*Emanuele Giallongo, Roma*  
*Andrea Grazian, ESO/Padova*

More details on the present project can be found in Saracco et al. (2001) and Vanzella et al. (2001).



#### References

- Bertin, E., Arnouts, S., 1996, *A&A*, 117, 393
- Casertano, S., de Mello, D., Dickinson, M., Ferguson, H. C., Fruchter, A. S., Gonzalez-Lopezlira, R. A., Heyer, I., Hook, R. N., Levay, Z., Lucas, R. A., Mack, J., Makidon, R. B., Mutchler, M., Smith, T. E., Stiavelli, M., Wiggs, M. S., Williams, R. E., 2000, *AJ*, 120, 2747
- Fernández-Soto, A., Lanzetta, K.M., Yahil, A., 1999, *ApJ*, 513, 34
- Madau, P., Pozzetti, L., 2000, *MNRAS*, 312, L9
- Moorwood, A.F.M., Cuby, J.G., Ballester, P., et al., 1999, *The ESO Messenger* 95,1
- Norris, R. P., Hopkins, A., Sault, R. J., Ekers, R. D., Ekers, J., Badia, F., Higdon, J., Wieringa, M.H., Boyle, B.J., Williams R. E., astro-ph/9910437
- Saracco, P., Giallongo, E., Cristiani, S., D'Odorico, S., Fontana, A., Iovino, A., Poli, F., Vanzella, E., 2001, *A&A* 375, 1S
- Vanzella, E., Cristiani S., Saracco, P., Arnouts, S., Bianchi, S., D'Odorico, S., Fontana, A., Giallongo, E., Grazian, A., 2001, *AJ*, 122, 2190
- Volonteri, M., Saracco, P., Chincarini, G., 2000, *A&AS*, 145, 111
- Williams, R. E., Blacker, B., Dickinson, M., Dixon, W. V. D., Ferguson H. C., Fruchter, A. S., Giavalisco, M., Gilliland, R. L., Heyer, I., Katsanis, R., Levay, Z., Lucas, R. A., McElroy, D., Petro, L., Postman, M., Adorf, H.-M., Hook, R. N. 1996, *AJ*, 112, 1335-1389
- Williams, R.E., Baum, S., Bergeron, L.E., Bernstein, N., Blacker, B.S., Boyle, B.J., Brown, T.M., Carollo, C.M., Casertano, S., Covarrubias, R., et al., 2000, *AJ*, 120, 2735

# FAINT GALAXY DETECTION IN DRIZZLED DATA

*Paul Bristow & Richard Hook*

The use of dithering — taking multiple images of the same field with small shifts between them - as a means of recreating image information lost by undersampling is well established. The Drizzle algorithm (Fruchter & Hook 2002) has become widely used as a robust method for combining such images. These techniques clearly enhance the spatial resolution of the final image when the input is undersampled, but the impact on the photometry of the output, particularly for extended objects, is hard to predict analytically. Up to now tests of the Drizzle software have mostly either utilised real data for which nothing was known about the underlying properties of the objects measured or simulated point-sources. Here we present some tests that compare photometry of drizzled and non-drizzled simulated deep field data to the known properties of the objects measured. The efficiency of detection of the faintest objects is also addressed.

## DRIZZLING

The Drizzle algorithm was invented to satisfy the image combination requirements of the Hubble Deep Fields and subsequently widely used for HST imaging data. It is a direct 'forward' method in which each input pixel is mapped on the output, taking into account geometric distortion and image shifts, and combined with the output in an optimally weighted manner. The input pixels are 'shrunk' before combination to minimise resolution loss without producing excessive variations of weight between output pixels, or in extreme cases missing data points. The method is described in full in Fruchter & Hook (2002).

## NUMERICAL UNIVERSE SOFTWARE

In an attempt to better understand the observational and selection effects that intervene between any model describing the underlying galaxy distribution and the numbers of objects that we count on the sky, a suite of simulation software has been developed. This software, which consists of a number of tasks collected together under the name "Numerical Universe" (NU), has many possible applications (see Bristow 1996).

The application discussed here is essentially a spin-off. Having incorporated dithering and drizzling into the simulations in order to mimic the processing of data in ultra-deep surveys such as the HDF, it was realised that this provided a controlled way of testing the effect of drizzling on detection and photometry.

## THE NU SOFTWARE

This is a brief overview of the main steps in the creation of NU simulations used here. A more complete description of the algorithms can be found in Bristow 1996 (see also Driver et al 1997).

- A volume of space is populated Monte Carlo fashion with galaxies following an input luminosity function and an evolutionary scheme.
- The galaxies are assigned spectra, surface brightness profiles and a range of rest-frame central surface brightnesses appropriate to their types.
- The K/extinction corrections are computed from the galaxy spectra, the filter response function and a redshift/wavelength/extinction model (a more sophisticated, though somewhat ad-hoc model that calculates the extinction from intervening clouds along the line of sight is also available).
- The corresponding apparent surface brightness profiles in the required band pass and the specified evolutionary model are calculated.
- Each galaxy is assigned a position on the sky (no clustering), an inclination, position angle and a simple two-dimensional structure.
- The galaxy images are mapped onto a two-dimensional array representing a CCD frame of the same resolution as a WFPC2 chip and stellar images are added.
- Sky noise, readout noise and gain are incorporated as appropriate for a survey of interest and the appropriate filter/detector combination.
- If a dithered and drizzled result is required then a similar frame may be created seven more times with offsets of all galaxy positions (for example, corresponding to the dither pattern used in HDF observations).
- If necessary (see previous step), the eight simulated frames are combined using the Drizzle task.
- SExtractor is used to extract and measure faint images (with parameters set to match a real catalogue of interest).
- The properties of the extracted objects are compared with the known intrinsic properties (known, that is, from the first three steps above). In this way it is not only possible to derive the  $n(m)$  and  $n(z)$ , but also to gain an insight into the way the observing process has affected the underlying distribution.

The same artificial sky can be observed with various filters and in this way colours can be added to the catalogues and spectroscopic redshifts can be compared with the known intrinsic redshift.

## TESTS

The NU software was used to simulate CCD exposures of deep fields. The observational parameters (aperture, filters, CCDs, sky levels, throughput, read noise) were similar to those of the HDF. The cosmology was the now standard  $\Omega_M = 0.3$ ,  $\Omega_\Lambda = 0.7$ ,  $H_0 = 70$  km/s/Mpc and the SEDs and LFs of the galaxy populations were taken from a model found to reproduce the counts from the HDF at a level acceptable for this work.

Two B band frames were produced, both containing exactly the same population of objects. Each effectively contained 80 1600s exposures. In the first case the exposures formed eight groups of ten perfectly aligned exposures while the pointings of the groups themselves were shifted relative to one another according to a dither pattern actually used for HDF-N. The exposures within the groups were simply stacked and the results from the groups were combined using the Drizzle software.

In the second case, all 80 exposures were exactly aligned and were simply stacked together, the IRAF task IMLINTRAN was then used to stretch and interpolate the frame to match the scale of the drizzled frame. This latter stage was necessary to allow the use of exactly the same parameters in the photometry software (e.g., the number of connected pixels above a given threshold, which could not be simply scaled as this would effect linear objects differently from those extended in two dimensions). Subsets of these two simulations are shown below in Figure 1.

Figure 2 shows two image sections illustrating the way that the drizzling helps in crowded fields. The circles mark detections made by SExtractor, on the drizzled frame (left) the group near the bottom is correctly resolved into three separate faint objects, whereas just two objects are found on the non-drizzled frame (right). Note also that one of the galaxies above has gone completely undetected on the non-drizzled frame.

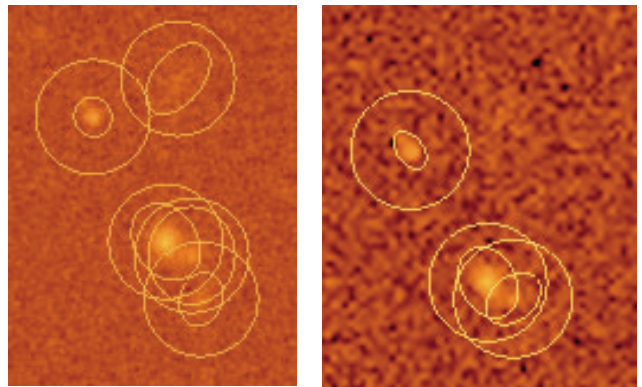


Fig 2: Detections in a crowded field.

SExtractor was used to detect and measure all objects containing 16 connected pixels more than  $2\sigma$  above the sky noise. Figure 3 shows the counts from the two frames compared to the known counts. Clearly neither match the known counts exactly (for exactly the observational reasons that the NU software was designed to investigate), but the drizzled frame does much better.

The average errors in the measured magnitudes in each magnitude bin were also investigated. We found little difference between the drizzled and non-drizzled results out to  $B = 27$ . At  $B = 27.5$  the drizzled frame performed somewhat better, but this is likely to be due only to the scarcity of detections made on the non-drizzled frame beyond  $B = 27$ .

Finally, the scatter plot in Figure 4 shows measured magnitude against known intrinsic magnitude for each object. The dispersion from  $x = y$  is similar for drizzled (black) and non-drizzled results (red). However, at fainter magnitudes the detections are simply not made on the non-drizzled frame in agreement with Figure 3.

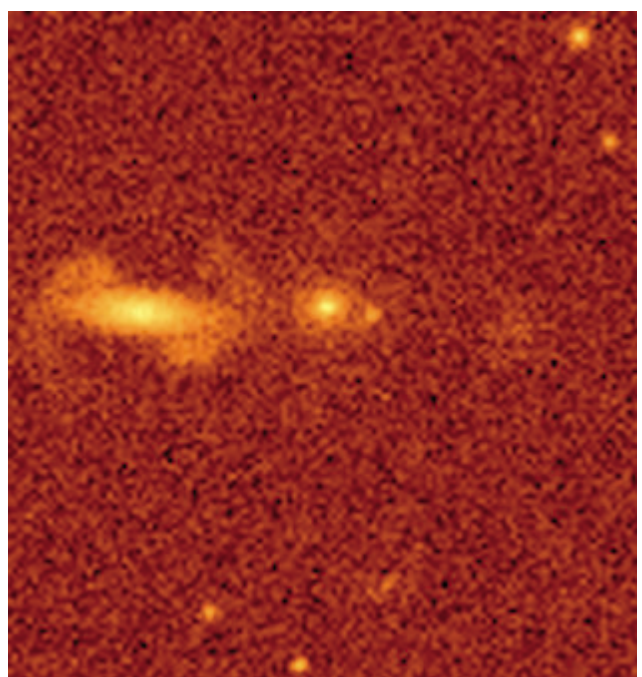
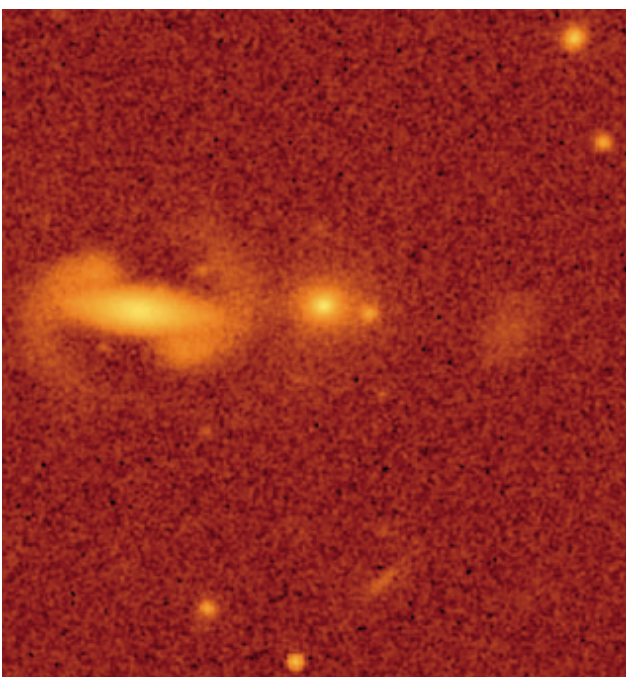


Fig 1: Sections taken from the two frames. Qualitatively the improved resolution of the drizzled frame (left) is immediately clear.

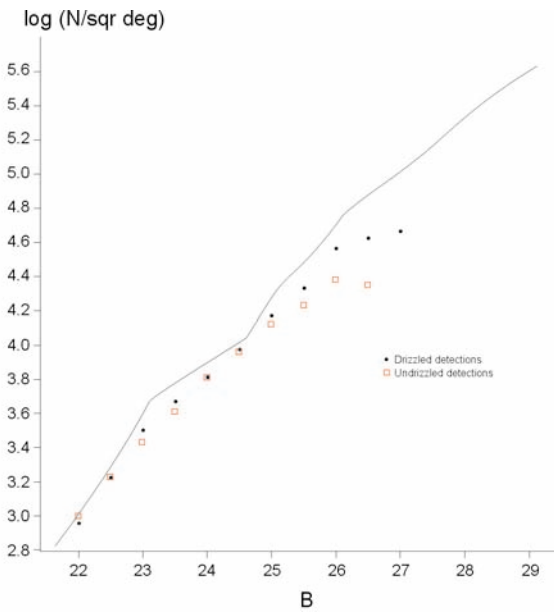


Fig 3: Number counts with drizzled and non-drizzled data.

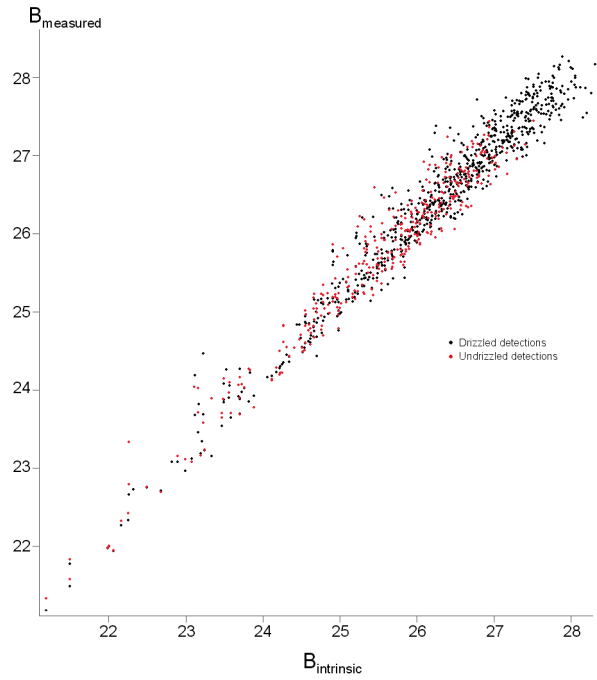


Fig 4: Measured versus known intrinsic B magnitudes.

### CONCLUSIONS

In summary, we find that the improved resolution achieved by employing a dithering strategy and recombining the data by drizzling can aid the detection of galaxies at faint magnitudes. The use of simulated data enables us to be sure that the increased detection rate is not due to increased spurious detections, but indeed reflects better quality data. Hence, number counts derived from drizzled data will require smaller corrections at the faint end. The use of drizzled data does not appear to affect the errors in photometry.

### References

- Fruchter A.S. & Hook, R.N., 2002, *PASP*, accepted - to appear in Feb 2002
- Bristow P. D., 1996, *PhD thesis, Wales Univ., Cardiff*
- Driver, S. P., Windhorst, R. A., Phillipps, S. & Bristow, P. D., 1996. *Astrophys. J.*, 461, 525.



### Painting with oxygen and hydrogen

This Hubble image shows the nebula NGC 2080, one of a chain of star-forming regions lying south of the 30 Doradus nebula in the Large Magellanic Cloud. These regions have been studied in detail with Hubble and have long been identified as unusual star-forming sites. 30 Doradus is the largest star-forming complex not only in the Large Magellanic Cloud, but also in the whole local group of galaxies.

This 'enhanced colour' picture is composed of three narrow-band filter images obtained with WFPC2 on 28 March 2000. The colours are red (ionised hydrogen, H $\alpha$ , 1040 seconds), green (ionised oxygen, 1200 seconds) and blue (ionised hydrogen, H $\beta$ , 1040 seconds). The image spans 67 x 67 arc-seconds, corresponding to 55 x 55 light-years at the distance of the Large Magellanic Cloud (168 000 light-years).

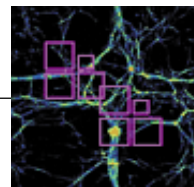
Read more at <http://hubble.esa.int> under "Releases" (heic0114)



Credit: ESA, NASA, & Mohammad Heydari-Malayeri (Observatoire de Paris, France)

## ENHANCED WFPC2 ASSOCIATIONS

*Alberto Micol & Daniel Durand (National Research Council, Canada, CADC)*



As part of a continuing effort to provide additional services to the astronomical community, and to allow astronomers to exploit the rich scientific contents of the archive more effectively, the ST-ECF and CADC have developed the concept of WFPC2 associations. This article describes the latest and most powerful form of this service.

Before February 1998 archive users had to retrieve WFPC2 observations on a single exposure basis. Because the necessary higher level of abstraction was missing from the archive, there was no simple way of recreating the observing strategy (eg, cosmic ray rejection, dithering) observers decided to employ, or which frames were associated with each other.

In February 1998 the ST-ECF introduced the first generation of WFPC2 associations, known as Type A associations. In the last few weeks, in November 2001, CADC and ST-ECF have released the second generation of associations, known as Type B. The meanings of these two terms and the advantages of the latter are described below.

The introduction of associations means that an archive user can browse through the WFPC2 archive and immediately see which exposures are aligned on the sky (CR-SPLIT), which exposures are dithered and by what extent (offsets).

Even when observers request well-aligned images these are sometimes subsequently found to be shifted by a small amount relative to each other. The associations describe what actually happened during the observing rather than the original intent.

An automatic pipeline that uses the additional association information has been put in place to allow WFPC2 archive researchers to retrieve not only On-The-Fly (OTF) re-calibrated exposures from the ST-ECF archive, but also other new products such as co-added Cosmic Ray free (CR) images.

### TYPE A ASSOCIATIONS

The telescope pointing information (jitter) is used to construct type A associations. If available the jitter provides a reliable way to identify CR-SPLIT observations, that is, observations split into two or more exposures to later remove the cosmic rays. Unfortunately, only about 57% of the WFPC2 observations have good accompanying jitter information. The rest either suffer from missing jitter information (telemetry dropouts) or a lack of accurate pointing information (e.g., no FINELOCK), or sometimes the telescope is found to have been slewing.

### TYPE B ASSOCIATIONS

To provide more complete associations a new scheme has been implemented. Type B associations contain all exposures following the same criteria used to select associations of Type A, regardless of the availability or the accuracy of the jitter information. The offsets between the various members of an association are now measured from the data themselves using a stan-

dard cross-correlation technique. When the cross-correlation fails (perhaps because there is not enough signal, typically a problem for images taken through blue filters), the jitter information is used. If the jitter information is missing or cannot provide reliable offsets, the science header World Coordinate System is used. In order to compute the relative shifts using cross-correlation techniques, many months of dedicated computer time were required.

### COMPARISON OF TYPE A AND B

When calibration observations (constituting ~30% of the whole archive, 21% if expressed in observing time) are excluded, the percentage of observations that end up in associations is 75% for Type A and 93% for Type B. The corresponding percentage of observations that not only end up in associations, but for which we also reliably know the offsets, is 57% for Type A and 93% for Type B. When expressed as total exposure times these numbers become:

Type A	Type B
29.6×10 <sup>6</sup> seconds	42.1×10 <sup>6</sup> seconds
66.4% of total scientific time	94.4% of total scientific time

As a result the Science Archive Facility can now provide automatically stacked (co-added and cosmic-ray free) products for the vast majority of images collected by WFPC2.

As an aside, it is interesting to note that a comparison of the Type A (jitter) and Type B (cross-correlation) shifts led to the discovery of a zero-point drift of the jitter pointing information. STScI subsequently confirmed the problem when they noted a similar drift during a 8-day continuous observation of 47 Tuc (Ron Gilliland and collaborators' search for planetary companions). Our plots showing the drift are available at [http://archive.eso.org/archive/hst/wfpc2\\_asn/jitter\\_drift/](http://archive.eso.org/archive/hst/wfpc2_asn/jitter_drift/)

### HOW ARE THE SHIFTS COMPUTED?

There are three possible methods to compute the shifts:

#### CROSS-CORRELATION:

The cross-correlation method (IRAF stsdas.analysis.dither package) should offer the most reliable offsets as it uses the pixels of the images themselves, not ancillary information from another source, and also offers an estimate of the error from the width of the cross-correlation peak. To ensure the validity of the measurements, two things are taken into consideration:

- The estimated shift error from the cross-correlation

b) Since the shifts of each individual WFPC2 chip are computed separately, a voting system is introduced to make sure that the intra-chip shifts agree.

#### WHAT IS AN ASSOCIATION?

An association is a logical group of exposures. The deepest of such exposures is called the leader of the association. The association identifier (asn\_id) is named after the leader, replacing the last character with the letter "B"

An exposure is associated to a given leader if:

- it belongs to the same programme (same proposal id)
- it was observed with the same filter (or combination of filters)
- its separation on the sky is not greater than 10 arcsec (100 WF4 pixels)
- the position angle does not differ by more than 0.03 degrees

These criteria do not prevent an exposure from belonging to two associations. To avoid this, when an exposure could be associated to two (or more) leaders, the closest one is chosen.

#### JITTER INFORMATION

For each observation, RA, DEC, ROLL measurements (averages and standard deviations) are extracted from the Observatory Monitoring System files, along with some of the telemetry keywords; the comparison of RA and DEC with those of the association leader provides the jitter offsets. The quality of the jitter is also evaluated. These offsets were used in the previous associations (associations of Type "A"). To find out more about jitter files, please see:

[http://archive.eso.org/archive/hst/wfpc2\\_asn/jitter.html](http://archive.eso.org/archive/hst/wfpc2_asn/jitter.html)

An example to illustrate the usefulness of jitter measurements can be found at:

[http://archive.eso.org/archive/hst/wfpc2\\_asn/jitter\\_examples.html](http://archive.eso.org/archive/hst/wfpc2_asn/jitter_examples.html)

#### IMAGE HEADER WCS INFORMATION

The WCS of each association member is compared with the WCS of the association leader (defined to be the deepest first observation in the group).

Of the three methods, preference is given to the cross-correlation algorithm. In those cases where the cross-correlation method fails (not enough signal, typically in blue filters or very short exposure times), the jitter information is used.

If the jitter information is missing or does not provide good offsets, the World Coordinate System (WCS) information is used.

#### HIGH-LEVEL DATA PRODUCTS

Associations trace back the observing strategy (CR-SPLIT, POS-TARG) adopted by observers. Such information is now offered via the archive web interface, changing the way the Archive Community browses the HST Mission Log. This has the advantage of making knowledge about what actually happened during the observations available.

Having measured the offsets among the members of associations, the archive users are offered an automatic pipeline to generate higher level products by application of the following processing steps:

□ On-The-Fly Re-calibration (OTF)  
OTF is applied to each individual exposure;

□ Association File Generation  
An association file, which describes the associations and its members, is generated from the database where all the shift parameters are stored;

□ Mosaicing, Cosmic Ray Rejection and Co-Addition  
By knowing the shifts among the exposures in the association (from the association file) an IRAF procedure is able to co-add the calibrated exposures on-the-fly. Cosmic ray removal is also taken care of if there are sufficient exposures.

The implementation currently uses the IMSHIFT and IM-COMBINE tasks within IRAF. At present we do not offer the drizzle algorithm.

#### WORK IN PROGRESS

The stacking procedure works well, but some changes are necessary to optimally handle images of extended objects. Another minor current deficiency is that weight maps are not yet provided for those associations having non-negligible shifts. An optimised stacking routine is currently being worked out and we aim to release it soon. These new steps are all options that may be switched on or off by the user.

Since the processing is completely automatic, the results cannot be perfect for all cases. As a quality assurance check, the user usually receives, in addition to association products, the individually calibrated images, as well as a file containing the relative shifts used to generate the association product. In this way, more precise assessment can be performed before starting any scientific analysis.

In the near future, a dedicated pipeline will start producing preview images of the WFPC2 mosaics, so that the archive users will be able to visually inspect the quality of the data, before archive request submission.

#### ACKNOWLEDGEMENTS

The Type B WFPC2 associations system has been developed jointly by ST-ECF and CADC (Canadian Astronomy Data Centre, part of the National Research Council of Canada using a grant from the Canadian Space Agency).



#### FURTHER INFORMATION

To learn more about WFPC2 associations, please refer to the following URLs:

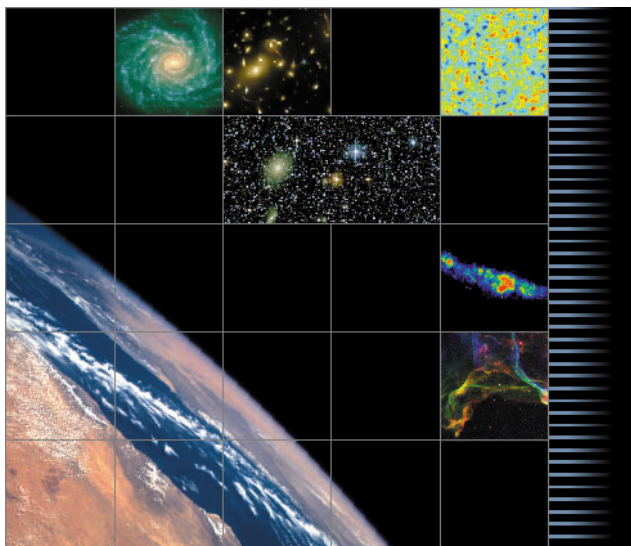
WFPC2 Associations Home Page:  
[http://archive.eso.org/archive/hst/wfpc2\\_asn/](http://archive.eso.org/archive/hst/wfpc2_asn/)  
Frequently Asked Questions:  
[http://archive.eso.org/archive/hst/wfpc2\\_asn/faq.html](http://archive.eso.org/archive/hst/wfpc2_asn/faq.html)  
Pipeline Products:  
[http://archive.eso.org/archive/hst/wfpc2\\_asn/wfpc2\\_products.html](http://archive.eso.org/archive/hst/wfpc2_asn/wfpc2_products.html)  
Idiosyncrasies&Warnings:  
[http://archive.eso.org/archive/hst/wfpc2\\_asn/faq.html#warnings](http://archive.eso.org/archive/hst/wfpc2_asn/faq.html#warnings)  
Jitter Zero Point Drift:  
[http://archive.eso.org/archive/hst/wfpc2\\_asn/jitter\\_drift/](http://archive.eso.org/archive/hst/wfpc2_asn/jitter_drift/)

ESO/ESA/NASA Astronomy Conference

## TOWARDS AN INTERNATIONAL VIRTUAL OBSERVATORY

<http://www.eso.org/vo2002>

Scientific Motivation, Roadmap for Development and Current Status



June 10 - 14, 2002, Garching, Germany

A **virtual observatory (VO)** is a collection of interoperating data archives and software tools that utilise the Internet to form a scientific research environment. A real observatory consists of telescopes, each with a collection of unique astronomical instruments, the VO consists of a collection of data centres each with unique collections of astronomical data, software systems and processing capabilities.

The development of a VO is driven by two key factors. Firstly, there is an explosion in the size of astronomical data sets delivered by new large facilities. The processing and storage capabilities necessary for astronomers to analyse and explore the forthcoming data sets will greatly exceed the capabilities of the desktop systems currently available. Secondly, a potential scientific gold mine remains unexplored and underexploited because large data sets in astronomy are unconnected. If large surveys and catalogues could be joined into a uniform and interoperating "digital universe", entire new areas of astronomical research would become feasible.

Major virtual observatory initiatives were launched in Europe and in the USA in the autumn of 2001. The Astrophysical Virtual Observatory (AVO) Project, funded by the European Commission, is a three-year study for the design and implementation of a virtual observatory for European astronomy. AstroGrid is a project aimed at building a data-grid for UK astronomy, which will form the UK contribution to a global Virtual Observatory. In the USA, the National Virtual Observatory (NVO) is a new project funded by a five-year Information Technology Research grant from the National Science Foundation.

This meeting will bring together a diverse community of scientists to discuss the relevant scientific and technological issues necessary to fully exploit the potential of the Virtual Observatory.

## CONTENTS

HST News and Status .....	2
NGST News .....	2
ACS Grism Calibration .....	4
Astronomy Exercise Series .....	7
HDF-S Deep IR Imaging .....	8
Galaxy Detection in Drizzled Images .....	11
Enhanced WFPC2 Associations .....	14

ST-ECF

### Head

Piero Benvenuti  
+49-89-320 06 290  
[Piero.Benvenuti@stecf.org](mailto:Piero.Benvenuti@stecf.org)

### Science Data and Software

Rudolph Albrecht  
+49-89-320 06 287  
[Rudi.Albrecht@stecf.org](mailto:Rudi.Albrecht@stecf.org)

### Science Instrument Information

Robert A.E. Fosbury  
+49-89-320 06 235  
[Robert.Fosbury@stecf.org](mailto:Robert.Fosbury@stecf.org)

### Public Outreach

(Hubble European Space Agency  
Information Centre):  
Lars L. Christensen  
+49-89-320 06 306  
[lars@stecf.org](mailto:lars@stecf.org)

The Space Telescope-European Coordination Facility  
Karl-Schwarzschild-Str.2  
D-85748 Garching bei München, Germany

### Website

<http://www.stecf.org>

### Telephone

+49-89-320 06 291

### Telefax

+49-89-320 06 480

### Hot-line (email)

[stdesk@stecf.org](mailto:stdesk@stecf.org)

### Email

<user>@stecf.org

### ST-ECF Newsletter

### Editor

Richard Hook, [Richard.Hook@stecf.org](mailto:Richard.Hook@stecf.org)

### Editorial assistant

Britt Sjöberg, [Britt.Sjoeborg@stecf.org](mailto:Britt.Sjoeborg@stecf.org)

### Layout, illustrations and production

Martin Kornmesser &  
Lars L. Christensen

### Printed by

Repro Schottenheim, München

### Published by

ST-ECF

